THE ASTROPHYSICAL JOURNAL, 422:467–479, 1994 February 20

CONSTRAINTS ON MOLECULAR GAS IN COOLING FLOWS AND POWERFUL RADIO GALAXIES

CHRISTOPHER P. O'DEA,[1] STEFI A. BAUM,[1] PHILIP R. MALONEY,[2]
LINDA J. TACCONI,[3] AND WILLIAM B. SPARKS[1]
Received 1993 April 5; accepted 1993 August 24

ABSTRACT

We searched for molecular gas in a heterogeneous sample of five radio-loud galaxies (three of which are inferred to be in cooling flow clusters) using the Swedish-ESO Submillimeter Telescope. We do not detect CO in emission in any of the cluster sources at a 3 σ level of typically 15 mK. White et al. (1991) have suggested that the apparent low-energy X-ray absorption toward cooling flow clusters is due to column densities of $N_H \sim 10^{21}$ cm^{-2} in these clusters with a spatial covering factor of order unity and a total mass of $M \sim 10^{12}$ $M_\odot$. Our limits are inconsistent with these column densities and spatial covering factor unless the molecular gas is very cold (kinetic temperature close to 2.7 K) or there only a few clouds along each line of sight. We calculate the heating by X-rays from the intracluster medium and derive constraints on the equilibrium temperatures of the molecular clouds. We estimate *minimum* temperatures in the range ~20–30 K. These calculations suggest that it is not possible to cool the clouds sufficiently to explain the nondetections of molecular gas as a result of low temperature (kinetic temperature close to 2.7 K).

We find that clouds of atomic and molecular hydrogen require strict fine-tuning of parameter space in order to satisfy the requirements for the large column densities $N_H \sim 10^{21}$ cm^{-2}, unit covering factor, and a small number of clouds along the line of sight. The combination of these constraints with the additional requirement that the optical depth in H I be very large is inconsistent with the clouds being atomic. Clouds of molecular hydrogen are not currently ruled out, but the range of parameter space is shrinking. Currently the only way molecular gas can be responsible for the X-ray absorption and still be consistent with our observations is if (1) there is of order one cloud along the line of sight and (2) the optical depth in ^{12}CO $1 \rightarrow 0$ is less than 10.

In addition, we present a VLA image of NGC 4696 which shows a diffuse radio morphology comparable to that of the dust lane and emission line complex and suggest this object is a member of the class of "amorphous cooling flow radio sources." The ^{12}CO $1 \rightarrow 0$ line is detected in emission in PKS 0634−206, a classical double radio galaxy which is rich in extended optical emission line gas. The estimated molecular gas mass is $M_{mol} \sim 3 \times 10^9$ $M_\odot$ and is much larger than that of the ionized component detected in Hα suggesting that the emission-line nebula is radiation bounded.

Subject headings: cooling flows — galaxies: ISM

1. INTRODUCTION

In the standard "cooling flow" models of the intracluster medium, hot (10^7–10^8 K) gas with a cooling time less than the Hubble time cools and falls quasi-hydrostatically into the center of the cluster potential well (e.g., Fabian, Nulsen, & Canizares 1984, 1991; Sarazin 1988). There, it is expected to be accreted by the central dominant galaxy of the cluster. Indeed, radial profiles of temperature and density in the intracluster gas inferred from X-ray imaging and X-ray spectroscopic observations, show unequivocally that cooler, denser gas (10^6–10^7 K) does exist in the centers of clusters (e.g., Fabian et al. 1981; Stewart et al. 1984; Canizares, Markert, & Donahue 1988; Mushotzky & Szymkowiak 1988; Mushotzky 1992; Böhringer et al. 1992). Typical mass accretion rates inferred in these cooling flow clusters are 100 $M_\odot$ year^{-1} within a region 100 kpc in radius. However, such large accretion rates immediately raise an as yet unsolved problem: determining the ultimate fate of the inflowing material. The total amount of mass detected in gas at temperatures less than 10^5 K in central dominant galaxies is less than 10^9 $M_\odot$, and the limit in the rate of star formation with a normal IMF is typically 0.1 times the X-ray–determined mass accretion rates. The lack of compelling evidence for the existence of cooling flows at any wavelength regime other than X-rays has led to considerable skepticism of the cooling flow model (e.g., Baum 1992; Sparks 1992).

Recently, White et al. (1991) reported the discovery of large amounts of cold X-ray–absorbing matter distributed over the inner few 100 kpc of some clusters of galaxies. The presence and distribution of this gas were inferred because the *Einstein Observatory* Solid State Spectrometer data require a significant excess absorption in addition to a cooling flow component in some clusters. Additional evidence for the presence of the X-ray–absorbing component comes from data obtained with the *Einstein* IPC (Wang & Stocke 1993), BBXRT (e.g., Mushotzky 1992; Miyaji et al. 1993), and *ROSAT* PSPC (Allen et al. 1993). White et al. (1991) applied simple arguments and came to the conclusion that the absorbing component was likely to be in the form of either atomic or molecular hydrogen. To produce the X-ray absorption observed, the cold gas must have a high spatial covering factor. However, to have avoided detection in the numerous searches for cold matter that have been conducted in recent years, the cold gas must (1) be very cold indeed and (2) have a very low covering factor in velocity space. White et al. (1991) estimate a total mass for the absorbing gas of

[1] Space Telescope Science Institute, 3700 San Martin Drive, Baltimore, MD 21218.
[2] JILA, Campus Box 440, University of Colorado, Boulder, CO 80309.
[3] Max-Planck-Institut für extraterrestrische Physik, Giessenbachstrasse, W-8046, Garching bei München, Germany.

$\sim 3 \times 10^{11}$–10^{12} $M_\odot$. This then constitutes a significant fraction of the total mass predicted to have cooled out of the cooling accretion flow during the lifetime of the cluster.

The presence of this cold gas has profound implications for our understanding of clusters. In addition, its ability to survive in the hot ICM for $\sim 5 \times 10^9$ yr has important implications for the strength and configuration of the magnetic field; thermal conduction and evaporation/ablation of the cold gas by the hotter surrounding medium must be suppressed. Clearly, a result as far-reaching as this one requires independent confirmation outside the X-ray spectral regime.

In this paper we report the results of a search for CO in three cooling flow clusters. We also report observations of two powerful radio galaxies in the which there is evidence that the host galaxy has acquired gas from a companion. We consider the effects of X-ray heating and estimate equilibrium temperatures for the molecular clouds in cooling flow clusters. We examine the effects of cloud temperature and covering factor on detectability of the clouds and generalize our discussion to include results from other searches.

2. SEST OBSERVATIONS AND REDUCTION

We searched for $J = 1 \rightarrow 0$ line emission of ^{12}CO in five radio galaxies (Table 1) and $J = 2 \rightarrow 1$ emission in one of the objects with the Swedish-ESO Submillimeter Telescope (SEST). At the redshifts of the sources, the CO $J = 1 \rightarrow 0$ line was expected at frequencies of 96–114 GHz, where the half-power beamwidth of the telescope is 43–51″. The observations were made in 1990 May. The telescope was equipped with dual polarization cooled Schottky receivers which covered frequency ranges of 80–116 GHz and 220–260 GHz. Typical total single-sideband system temperatures were 400–700 K. A detailed description of the SEST is given by Booth et al. (1989).

The CO data were obtained by switching between two beams symmetrically displaced to each side of the telescope axis and separated by 4′ on the sky. Pointing was checked every 2–3 hr by making observations of SiO masers and planets, and the overall pointing accuracy is estimated to be $\sim 7''$. Antenna temperatures (T_A^*) were calibrated using a standard chopper wheel technique, switching between sky and an ambient load, which corrects for first-order atmospheric losses and ambient temperature losses (Ulich & Haas 1976; Kutner & Ulich 1981). The CO intensities quoted in this study are main beam brightness temperatures (T_{mb}), which are the calibrated antenna temperatures divided by the main beam efficiency η_{mb} (see Downes 1989). For the SEST, η_{mb} at 110 GHz was 0.74 and 0.54 at 230 GHz. To convert the data to the T_R^* scale (Kutner & Ulich 1981), an efficiency due to forward scatter and spillover $\eta_{fss} = 0.92$ should be used, where $T_R^* = T_A^*/\eta_{fss}$. Relative calibration uncertainties are estimated to be about 10%. Velocity resolution was provided by a broadband acousto-optical spectrometer which was split to accept both polarizations. The total bandwidth available for each polarization was 500 MHz (1300 km s^{-1}) with a spectral resolution of 0.7 MHz (1.8 km s^{-1}) per channel. The data were further reduced off-line using the DRAWSPEC data reduction package developed by Harvey Liszt at NRAO. To improve the signal-to-noise ratio of the data, the spectra were boxcar-smoothed to final velocity resolutions of 5–10 km s^{-1}, giving an rms noise level of $\sim$4–7 mK (T_{mb}). Since beam-switching produced spectra with fairly flat baselines, removal of linear or second-order polynomials from the data was generally sufficient.

3. SEST RESULTS

A summary of the observational parameters and basic results are presented in Table 2. We assume $H_0 = 75$ km s^{-1} kpc^{-1} and $q_0 = 0.1$ throughout. The derived parameters are calculated in the following way.

For the nondetections, the 3 σ upper limit to the flux integral (the integrated CO line intensity) is given by

$$W_{CO} = 3\,\sigma_c\,V_{line}\left(\frac{v_{chan}}{V_{line}}\right)^{1/2} \text{K km s}^{-1} \quad (1)$$

where σ_c is the channel-to-channel rms noise, v_{chan} is the smoothed velocity channel spacing, and V_{line} is the width of the line (with a rectangular profile assumed for simplicity). This is a good approximation since, if the line is Gaussian, the correct line integral is obtained with $V_{line} \simeq 1.06$ FWHM.

In our Galaxy, the ^{12}CO $1 \rightarrow 0$ is optically thick and an empirical relationship between CO flux integral and column density of molecular hydrogen N_{H_2} has been derived,

$$N_{H_2} \simeq 2.8 \times 10^{20} W_{CO}\ \text{cm}^{-2} \quad (2)$$

(e.g., Bloemen et al. 1986; Scoville & Sanders 1987; Young & Scoville 1991), though its application to other galaxies is controversial (e.g., Maloney & Black 1988; Sage & Isbell 1991). We adopt this conversion here with the implicit understanding that the resulting column densities are highly uncertain.

The total mass of molecular hydrogen within the SEST observing beam is given by integrating spatially over the Gaussian beam giving

$$M_{mol} = \frac{\pi r^2}{4 \ln 2} N_{H_2} m_{H_2} \quad (3)$$

where m_{H_2} is the mass of the hydrogen molecule and r is the HWHM of the SEST beam at the distance of the source.

TABLE 1

SOURCE LIST

Source (1)	Other Name (2)	R.A. (B1950.0) (3)	Decl. (B1950.0) (4)	References (5)	$z_\odot$ (6)	References (7)	D_{lum} (Mpc) (8)	Scale (kpc arcsec^{-1}) (9)
0634−206.....	...	06^{h}34^{m}23^s.27	−20°32′18″.5	1	0.056	1	230	1.0
0745−191.....	...	07 45 18.45	−19 10 11.6	1	0.1028	1	430	1.7
0915−118.....	3C 218	09 15 41.20	−11 53 04.9	1	0.0547	4	217	1.0
1246−410.....	NGC 4696	12 46 03.49	−41 02 17.8	2	0.0106	5	43	0.2
1934−638.....	...	19 34 47.59	−63 49 37.8	3	0.183	3	791	2.7

REFERENCES.—(1) Baum et al. 1988 and references therein; (2) Our VLA core position; (3) Fosbury et al. 1987; (4) Smith & Heckman 1989; (5) Dawe et al. 1977; Davies et al. 1987.

TABLE 2

OBSERVATIONAL PARAMETERS AND RESULTS

Source[a] (1)	Time[b] (minutes) (2)	σ_c[c] (mK) (3)	Velocity Resolution[d] (km s^{-1}) (4)	v_{corr}[e] (km s^{-1}) (5)	W_{co}[f] (K km s^{-1}) (6)	$T_R c_R$[g] (mK) (7)	M_{mol}[h] ($M_\odot$) (8)	Notes[i] (9)
0634−20.....	280	3.7	9.58	16321	0.71 ± 0.14	0 ± 1	3×10^9	1
0745−19.....	188	4.3	10.00	29236	<0.57	0 ± 1	$<8 \times 10^9$	
0915−11.....	152	5.0	9.55	15472	<0.66	20 ± 4	$<2 \times 10^9$	
0915−11.....	152	5.0	7.64	15524	−0.41 ± 0.14	20 ± 4	...	2
1246−41.....	208	5.2	9.16	2900	<0.66	0 ± 1	$<7 \times 10^7$	
1246−41.....	144	14	11.0	2908	<1.80	0 ± 1	$<2 \times 10^8$	3
1934−63.....	232	7.1	10.73	49892	<0.99	6 ± 1	$<5 \times 10^{10}$	

[a] Source name.
[b] Total integration time in minutes.
[c] Channel-to-channel rms of the main beam temperature T_{mb}.
[d] Smoothed velocity channel width in km s^{-1}.
[e] Relativistically correct velocity v_{corr} of the center of the central channel of the spectrum

$$v_{corr} = \frac{f_0^2 - f^2}{f_0^2 + f^2} c,$$

where c is the speed of light, z is the redshift, f_0 is the rest frequency of the CO transition, and f is the redshifted frequency $f = f_0/(1 + z)$.
[f] Integrated CO line intensity ($\int T_{mb}\, dV$) in K km s^{-1}. Upper limits are 3 σ, assume a velocity width of 200 km s^{-1} (for a rectangular line profile) and are calculated using eq. (1).
[g] Main beam brightness temperature of the continuum radio emission T_R weighted by the covering factor of the radio source within the SEST beam c_R.
[h] Mass of molecular gas calculated using eq. (4) and assuming a covering factor of unity.
[i] NOTES.—(1) Emission; (2) absorption; (3) $J = 2$–1 transition.

Putting the expression for the mass in a more useful form gives

$$M_{mol} = 10.60 \theta^2_{arcsec} D^2_{Mpc} N_{H_2-20}\, M_\odot \quad (4)$$

where θ is the SEST beam FWHM, D_{Mpc} is the luminosity distance in Mpc, and N_{H_2-20} is the column density in units of 10^{20} cm^{-2}. Values or 3 σ upper limits for the mass of molecular gas are given in Table 2 and range from $7 \times 10^7\ M_\odot$ in NGC 4696 to $5 \times 10^{10}\ M_\odot$ in PKS 1934−634.

The apparent optical depth of any CO seen in absorption against the continuum radio source is given by

$$\tau = -\ln\left(1 - \frac{\Delta T}{T}\right), \quad (5)$$

where ΔT is the depth of the line and T is the Rayleigh-Jeans brightness temperature of the radio continuum.

In the case where the CO is not detected, we estimate a limit on the covering factor c_f of the molecular hydrogen within the SEST beam assuming the CO is optically thick using the following simplified picture. Recall that our observational technique includes beam switching between the ON (source) position and OFF position in order to remove the contribution of the atmosphere to our spectra. Here we assume that the atmosphere is correctly removed and we consider only "astronomical" contributions to our observed spectra. The measured brightness temperature in the OFF position spectrum contains only the microwave background with Rayleigh-Jeans radiation temperature T_{bkg}. The measured brightness temperature in the ON position spectrum contains a contribution from the microwave background: $T_{bkg}(1 - c_f) + T_{bkg} c_f e^{-\tau}$, and a contribution from the CO which has Rayleigh-Jeans radiation temperature T_{CO}: $T_{CO}\, c_f(1 - e^{-\tau})$, where τ is the optical depth of the CO. For our purposes we can neglect the contribution from the continuum radio source since it is typically less than a few mK (see Table 2). We subtract the OFF spectrum from the ON spectrum, divide by the OFF spectrum, combine terms, and obtain

$$\frac{\text{ON} - \text{OFF}}{\text{OFF}} = \frac{c_f(1 - e^{-\tau})(T_{CO} - T_{bkg})}{T_{bkg}}. \quad (6)$$

The maximum measureable difference in the spectrum is between the baseline ($\tau = 0$) and the peak of the line ($\tau \gg 1$) and is given by $3\ \sigma_c = c_f(T_{CO} - T_{bkg})/T_{bkg}$, where 3 σ is our upper limit on the height of the CO line. Inverting for the covering factor gives

$$c_f \lesssim \frac{3\ \sigma_c\ T_{bkg}}{T_{CO} - T_{bkg}}. \quad (7)$$

4. DISCUSSION OF RESULTS FOR INDIVIDUAL SOURCES

Except for the following, our results are nondetections: (1) we detect ^{12}CO 1 → 0 in emission in PKS 0634−206, a classical double radio galaxy which is rich in extended optical emission-line gas and (2) we detect two blueshifted ^{12}CO 1 → 0 absorption features at the ~2 σ level toward Hydra A (3C 218), a powerful radio galaxy in a cooling flow in the poor cluster Abell 780. Below we discuss the significance and implications of the results for the individual sources. Gaussian fits to the detections are given in Table 3.

4.1. *0634−206*

0634−206 is a powerful, classical double radio galaxy with a total extent of ~870 kpc with a complex, filamentary emission line nebulae extending ~20″ (~20 kpc) from the galaxy nucleus (e.g., Schilizzi & McAdam 1975; Fosbury et al. 1984; Kronberg, Wielebinski, & Graham 1986; Hansen, Nørgaard-Nielsen, & Jørgensen 1987; Baum et al. 1988; Hansen 1989; Baum, Heckman, & van Breugel 1990). The kinematics of the emission-line gas appear to be dominated by rotation, with a (projected) rotational velocity of ~270 km s^{-1}. However, some nonsystematic motions (indicative of infall or outflow?) appear to be present (Tadhunter, Fosbury, & Quinn 1989;

TABLE 3

GAUSSIAN FITS TO THE DETECTIONS

Source[a] (1)	Peak[b] (mK) (2)	FWHM[c] (km s^{-1}) (3)	Center v_{corr}[d] (km s^{-1}) (4)	Center cz[e] (km s^{-1}) (5)	$V_g - V_{CO}$[f] (km s^{-1}) (6)	Notes[g] (7)
0634−20.....	6.8 ± 4.1	94 ± 60	16096 ± 26	16552	+220 ± 326	1
0915−11.....	−14.9 ± 6.8	28 ± 16	15604 ± 7	16032	+347 ± 37	2
0915−11.....	−14.9 ± 9.5	17 ± 13	15778 ± 5	16216	+173 ± 35	2

[a] Source name.
[b] Peak of the Gaussian in units of main beam brightness temperature (mK).
[c] Full width to half-maximum.
[d] Center heliocentric velocity, v_{corr} (see Table 2 for the definition).
[e] Center heliocentric velocity, cz, given to ease comparison with other work.
[f] The difference between the galaxy velocity and the CO velocity. Positive values are blueshifted and are motions away from the galaxy.
[g] NOTES.—(1) Emission; (2) absorption.

Baum et al. 1990). Baum, Heckman, & van Breugel (1990, 1992) have suggested that the emission line gas was tidally acquired.

Figure 1 shows that we have detected CO in emission. The flux integral is 5 σ above the noise. The line is resolved, though the signal-to-noise ratio is not high enough for the FWHM to be accurately determined (see Table 3).

The SEST beam has a FWHM of 47".5 which is comparable to the total extent of the emission-line nebula. The total mass in molecular gas is roughly $M_{mol} \sim 3 \times 10^9\ M_\odot$. We note that similar masses have been found in other powerful radio galaxies (e.g., Mazzarella et al. 1993). Baum & Heckman (1989) estimate the total mass of the Hα-emitting gas to be $M_{ionized} \sim 3 \times 10^9 f\ M_\odot$, where ($f$) is the volume filling factor of the ionized gas. When measured, the volume filling factor in 10^4 K gas tends to be in the range 10^{-4} to 10^{-6} (e.g., van Breugel 1988; Baum 1992). Thus, we find that the mass in molecular gas is likely to be much greater than that of the warm gas, suggesting that the emission-line nebula is radiation- (and not matter-) bounded. Our detection of this large amount of molecular gas is consistent with the hypothesis that $\sim 10^9\ M_\odot$ of cold material was acquired from a gas-rich galaxy, e.g., a spiral galaxy. The detection of larger amounts of molecular rather than ionized gas is consistent with a model for the emission-line clouds in which they are the thin ionized skins of dense molecular clouds. Clearly, it will be of interest to search for molecular gas in other radio galaxies with extended emission-line nebulae.

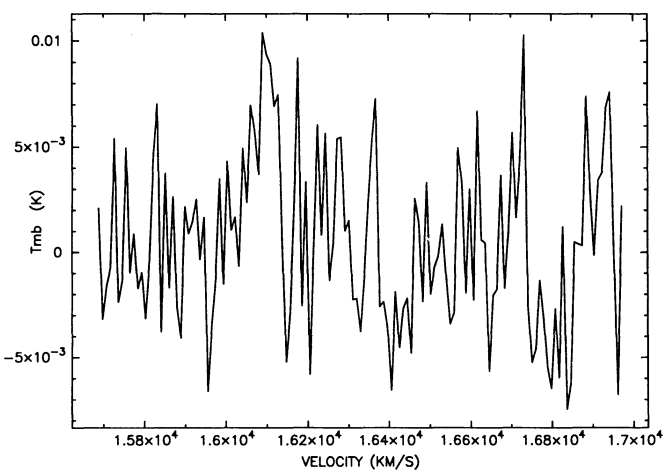

FIG. 1.—0634−206. SEST spectrum showing the detection of ^{12}CO 1 → 0 in emission.

4.2. *PKS 0745−191*

PKS 0745−191 is a powerful radio source with an amorphous and filamentary morphology (Baum & O'Dea 1991) embedded in one of the largest known cooling flows, $\dot{M} \sim 500\ M_\odot\ \mathrm{yr}^{-1}$ (Fabian et al. 1985; Arnaud et al. 1987). The extended emission-line nebula is one of the most luminous known in a cooling flow (e.g., Romanishin 1987; Johnstone, Fabian, & Nulsen 1987; Baum et al. 1988; Heckman et al. 1989). At the redshift of this source, our observing beam FWHM corresponds to 85 kpc. This is well within the cooling radius of the cluster, though it is larger than the observed extent of the emission-line nebula ~23 kpc. Our upper limit on the total mass of molecular gas within our observing beam is $M_{mol} \lesssim 8 \times 10^9\ M_\odot$.

This is strictly a limit on the amount of gas with FWHM $\lesssim$650 km s^{-1} (i.e., Doppler-broadened line width which is no more than about half of our total velocity bandwidth of 1300 km s^{-1}). However, our detection in 0634−206 has a FWHM of ~100 km s^{-1} (Table 3) and the detection of NGC 1275 has a FWHM of ~270 km s^{-1} (Mirabel et al. 1989; Lazareff et al. 1989). Unless 0745−191 is very different from these two objects, it seems unlikely that we could have missed the CO because the line widths are too broad.

4.3. *0915−11, Hydra A, 3C 218*

Hydra A is a powerful radio source associated with a cD galaxy in Abell 780 (e.g., Baum et al. 1988; Taylor et al. 1990). The cluster is a luminous X-ray source and appears to have a cooling flow with a large mass accretion rate $\dot{M} \sim 400\ M_\odot$ per year (David et al. 1990, converted to our value of the Hubble constant). The radio source also exhibits extremely high Faraday rotation measures with values of several thousand rad m^{-2} (Kato et al. 1987; Taylor et al. 1990; Taylor & Perley 1993). The galaxy possesses a system of emission-line filaments with a global S-shaped morphology and a maximum observed extent of ~15" (14 kpc) (Baum et al. 1988; Hansen 1989). The S-shaped morphology of the emission-line gas combined with the rapidly rotating "disklike" feature centered on the nucleus (Simkin 1979), and the emission-line "bridge" between the nucleus and a secondary nucleus to the SE has led Hansen (1989) to suggest that the emission-line gas has been tidally acquired.

Our SEST beam has a linear resolution of 45 kpc. We do not detect any CO in emission or absorption at the velocity of the cD (Fig. 2). However, because the cD velocity is offset to near

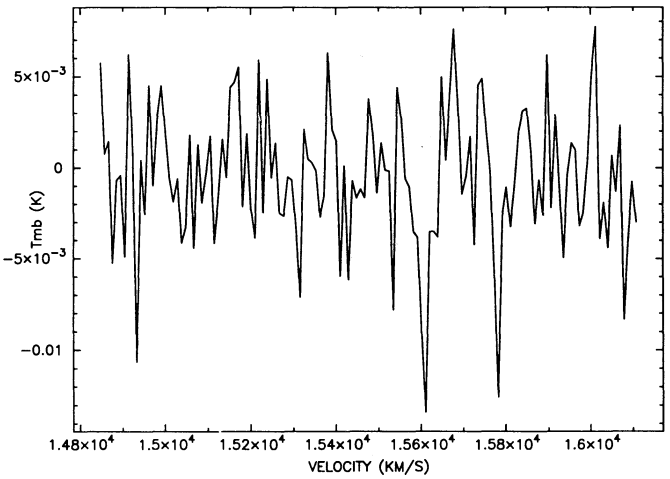

FIG. 2.—Hydra A (0915−11). SEST spectrum showing the marginal detection of two blueshifted ^{12}CO $1 \rightarrow 0$ features in absorption against the continuum radio source. A DC level of 20 mK has been subtracted from the spectrum.

the red edge of our spectrum, we are not sensitive to weak broad features with FWHM $\gtrsim 100$ km s^{-1}. Our upper limit corresponds to a limit on the mass of $M_{\rm mol} \lesssim 2 \times 10^9\ M_\odot$.

G. B. Taylor (1992, private communication) detects H I absorption in a 45″ beam toward the core and inner hot spots of Hydra A at velocity $cz \simeq 16{,}261$ km s^{-1}. Note that the resolution of the SEST at 115 GHz and the VLA at 21 cm in the D-configuration are similar. We very tentatively detect at the 2 σ level two features in absorption against the radio continuum source (see Table 3). We see such negative features only in Hydra A which has a Rayleigh-Jeans continuum brightness temperature of 20 mK, by far the largest in our source list (see Table 2). McNamara & Jaffe (1993) also report a possible 2 σ detection of an absorption feature toward Hydra A in their $J = 2 \rightarrow 1$ data at velocity $cz \simeq 16{,}110$ km s^{-1}. The velocity of the McNamara & Jaffe possible absorption feature does not agree with any of our two features, but instead falls between our features. The lack of agreement in velocity among Taylor's H I line, our two possible $J = 1 \rightarrow 0$ lines, and the possible McNamara & Jaffe $J = 2 \rightarrow 1$ line suggests that either (1) all three of the tentative CO features are spurious or (2) there is a system of very weak CO absorption features.

At 90 GHz, the total flux density within our observing beam is $S \sim 0.65$ Jy and is dominated by only three components of the radio source, the core and the two inner hotspots, with roughly equal flux densities (based on an extrapolation from 8 and 15 GHz; Taylor et al. 1990; G. B. Taylor 1992, private communication). Thus, if the CO absorption features are real, the absorbing material must lie in front of one or more of these radio components. The inferred optical depths for both of our possible absorption features (from eq. [5]) is $\tau \sim 1.4$ assuming that the material covers all the bright radio emission. If instead the absorbing material lies in front of only one or two of the three radio components, then the required optical depth will be higher. From equation (10), the thermal line width is FWHM ~ 0.18 km s^{-1} for a kinetic temperature of 20 K, while the observed line widths are $\sim$20–30 km s^{-1} (Table 3). Thus, the observed line width implies the existence of many clouds along the line of sight or a single, very turbulent cloud complex. We have inspected the broad-band and emission-line CCD images of Hydra A from Baum et al. (1988) for a clue as to the identity of the absorbing clouds. There are no visible galaxies or emission-line gas at the location of the two hotspots. Thus, the nature of the CO absorption features is unknown, though they could be produced in undetected galaxies or in molecular clouds in the ICM. Confirmation of these tentative detections is important.

4.4. *1246−41, NGC 4696*

NGC 4696 is the central dominant galaxy in the Centaurus cluster of galaxies. It has been suggested that there is a cooling flow in this cluster which deposits about 20 $M_\odot$ per year (Fabian et al. 1982a; Matilsky, Jones, & Forman 1985; Canizares et al. 1988; Thomas, Fabian, & Nelson 1987—converted using our adopted distance). This mass accretion rate over a period of 10^9–10^{10} yr would be expected to deposit $\sim 2 \times 10^{10}$–$10^{11}\ M_\odot$ of gas in the cluster center. We note that using the Parkes telescope with a 14′ beam, Jenkins (1983) placed an upper limit on the mass of optically thin atomic hydrogen in NGC 4696 of $M_{\rm H\,I} \lesssim 5 \times 10^8\ M_\odot$. The galaxy has a prominent "boomerang-shaped" dust lane with an angular size of roughly 20″ × 3″ and an emission-line nebula of similar dimensions (e.g., Fabian et al. 1982a; Jorgensen et al. 1983; Norgaard-Nielsen & Jorgensen 1984; Jedrzejewski 1985; Sadler 1987; Johnstone et al. 1987; Sparks, Macchetto, & Golombek 1989). Sparks et al. (1989) and de Jong et al. (1990) have independently suggested that there is no cooling flow in NGC 4696 and instead the evaporation of dust in the dust lane and/or in the galaxy is responsible for cooling the X-ray–emitting gas and mimicking the appearance of a cooling flow (but see also Canizares et al. 1993).

Our SEST beam FWHM for the $1 \rightarrow 0$ transition corresponds to 9.2 kpc at our adopted distance of NGC 4696 (43 Mpc for our Hubble constant). Based on extinction and emission-line maps of the dust lane, Sparks et al. suggest that the gas and dust are well mixed and the dust exhibits a Galactic extinction law. They estimate an associated gas mass for the dust lane of $\gtrsim 2 \times 10^7\ M_\odot$ where we have converted to our adopted distance to NGC 4696. De Jong et al. suggests that most of the dust in NGC 4696 is in a diffuse distribution of molecular clouds (total mass of molecular gas $M_{\rm mol} \sim 2 \times 10^9\ M_\odot$) with a radius of 10 kpc (roughly twice the FWHM of the SEST beam), and that only about 10% of the dust in NGC 4696 is contained in the dust lane. Based on our upper limit in the $1 \rightarrow 0$ transition we estimate an upper limit to the mass of molecular gas of $M_{\rm mol} \lesssim 7 \times 10^7\ M_\odot$ within the SEST beam. Thus, the molecular gas content of the dust lane estimated by Sparks et al. and the scenario suggested by De Jong et al. (with most of the gas outside the SEST beam) are consistent with our data.

We also observed NGC 4696 in the $2 \rightarrow 1$ transition but failed to detect it. The SEST beam is a factor of 2 smaller at this higher frequency, so we give the constraints for this smaller region adopting a conservative $(2 \rightarrow 1)\,(1 \rightarrow 0)$ intensity ratio of unity. The mass in molecular gas is then $M_{\rm mol} \lesssim 2 \times 10^8\ M_\odot$.

Our relatively low limit on the molecular gas mass ($\sim 10^8\ M_\odot$) is consistent with the "warming" or "evaporation" models for the X-ray emission. It is inconsistent with the $\sim 2 \times 10^{10}$–$10^{11}\ M_\odot$ of accreted gas expected naively in the standard "cooling flow" scenario unless another sink for the gas exists (e.g., low-mass star formation: Fabian, Nulsen, & Canizares 1982b; Sarazin & O'Connell 1983; White & Sarazin 1987; Westbury & Henriksen 1992) or less than 10^{-3} of the cooling gas ultimately reaches the central galaxy. See also the caveats discussed in § 5.

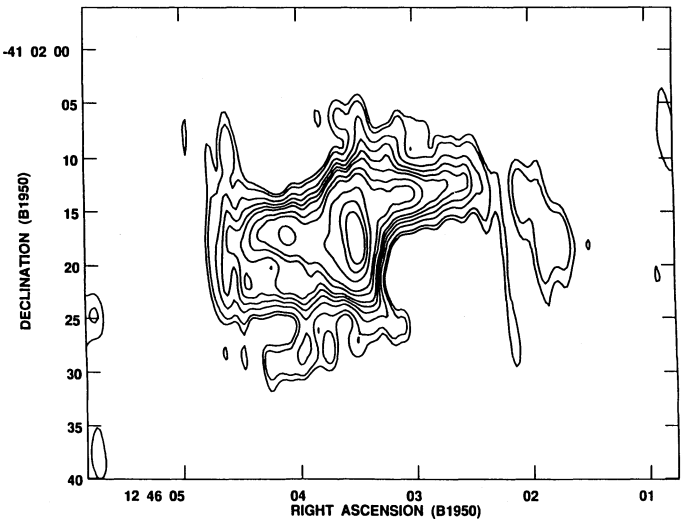

FIG. 3.—1246−41 (NGC 4696). VLA image at 1.4 GHz showing the amorphous radio morphology. The contour levels are −8.0, 8.0, 10.0, 15.0, 20.0, 25.0, 30.0, 40.0, 50.0, 75.0, 100.0, and 125.0 mJy per beam. The clean beam is 3.″6 × 1.″1 at 9.°4.

4.4.1. *VLA Image of NGC 4696*

Although NGC 4696 is a bright extended radio source (e.g., Harnett 1987; Sadler, Jenkins, & Kotanyi 1989) there are no published radio images. Since this is the only one of the sources discussed in this paper which does not have a published radio image, we present one here. We observed NGC 4696 with the VLA[4] as part of a study of the radio properties of central dominant galaxies in cluster cooling flows (see O'Dea & Baum 1986). We obtained snapshot observations at 20 cm with a subarray containing about half of the antennas in the A configuration on 1986 February 26. The data were calibrated, cleaned, and self-calibrated in the standard way within AIPS.

The resulting VLA image is shown in Figure 3. The total flux density in the image is about 3 Jy. Our *uv* coverage is sparse and there is large scale emission with about 1–2 Jy in flux density which is detected on short baselines, but which is not apparent in our image. Thus, this image is only a rough representation of the brighter, more compact radio features of the source.

The radio morphology source is diffuse and amorphous and is dominated by an overall Z shape though there are additional filamentary structures. The total extent visible in our image is about 25″. The overall shape and extent of the radio source (in this image) are comparable to that of the dust lane and emission-line filament system. Thus it would appear that there is an interconnection between the radio plasma, the dust lane, and the 10^4 K emission-line gas, though at this point it is not clear what the exact relationship is.

O'Dea & Baum (1986) and Burns (1990) noted that radio sources in cooling flows tend to have distorted or amorphous morphology. In addition, Baum & O'Dea (1991) suggested that many of the properties of PKS 0745−191, including its amorphous radio morphology, are due to the location of the radio source at the center of the rich, dense ICM with an inferred cooling flow. We suggest that NGC 4696 is also a member of this class of amorphous "cooling flow" radio sources. Other examples include 3C 317 (e.g., Baum et al. 1988; Burns 1990; Zhao et al. 1993), 3C 84 (e.g., Noordam & de Bruyn 1982; Pedlar et al. 1990; Burns et al. 1992), and 2A 0335+096 (Baum, O'Dea, & Sarazin 1984.

[4] The Very Large Array is operated by the National Radio Astronomy Observatory which is operated by Associated Universities, Inc., under cooperative agreement with the National Science Foundation.

4.5. *1934−638*

The radio structure of 1934−638 consists of a small double radio source with separation ∼42 mas (∼112 pc) (Tzioumis et al. 1989) making it one of the "compact double" radio sources (e.g., Phillips & Mutel 1982; Hodges & Mutel 1987). The radio spectrum has a simple convex shape peaking near 1.4 GHz (e.g., Kellerman 1966; Wills 1975; Kuhr et al. 1981; Tzioumis et al. 1989); thus, it is also one of the GHz peaked-spectrum (GPS) radio sources (e.g., Peacock & Wall 1982; Gopal-Krishna, Patnaik, & Steppe 1983; Fanti et al. 1990; O'Dea, Baum, & Stanghellini 1991). O'Dea et al. (1991) have suggested that GPS radio galaxies contain very dense and clumpy circumnuclear regions which tightly confine the radio source and restrict its expansion. Optical CCD images and spectra suggest that PKS 1934−638 is interacting with a companion (Heckman et al. 1986; Jauncey et al. 1986; Fosbury et al. 1987).

This source has the largest redshift of the five we have studied, and our observing beam FWHM is also very large (∼146 kpc). Thus, the limit of $M_{\rm mol} \lesssim 5 \times 10^{10}\ M_\odot$ that we place on the mass of molecular gas is not very restrictive.

5. CONSTRAINTS ON GAS IN COOLING FLOWS

5.1. *Molecular Hydrogen*

The properties of the warm $T \sim 10^4$ K clouds in the ICM have been discussed by, e.g., Loewenstein & Fabian (1990) from a theoretical point of view and by Baum (1992) from an observational point of view. The properties of putative cooler clouds have been discussed by Loewenstein & Fabian (1990), Jaffe (1992), Fabian (1992), and by White et al. (1991). White et al. have suggested that the apparent low-energy X-ray absorption toward cooling flow clusters is due to column densities of $N_{\rm H} \sim 10^{21}$ cm^{-2} in these clusters. They suggest the gas is distributed in cold, optically thick clouds (see also Loewenstein & Fabian 1990) with a spatial covering factor of order unity and corresponds to a total mass of $M \sim N_{\rm H} \pi R^2 m_{\rm H} \sim 10^{11}$–$10^{12} R_{100}^2\ M_\odot$ of gas, where R_{100} is the radius of the cooling region in units of 100 kpc and $m_{\rm H}$ is the mass of a hydrogen atom.

Considerable effort has also gone into detecting molecular gas in cooling flows. So far 24 clusters have been searched but not detected in CO (this paper; Jaffe 1987; Bregman & Hogg 1988; Grabelsky & Ulmer 1990; McNamara & Jaffe 1993; Antonucci & Barvainis 1993). Antonucci & Barvainis (1993) used a very wide bandwidth to search for very broad lines. O'Dea & Baum (1987) also searched for OH in absorption toward NGC 1275 with negative results. Here we discuss the constraints the CO observations place on the molecular component of the ICM. We give our derived constraints for the sample of 24 clusters in Table 4.

Equation (6) shows that the signal in our spectrum can be considerably reduced if the covering factor of the gas is very low. The covering factor can be decomposed into two parts: $c_f \sim c_{\rm spatial} c_{\rm vel}$, where $c_{\rm spatial}$ is a purely spatial covering factor which is required to be of order unity by the X-ray observations and $c_{\rm vel}$ is a covering factor in velocity

$$c_{\rm vel} \sim \frac{N_{\rm los}\, \Delta V_{\rm cloud}}{\Delta V_{\rm ensemble}}\,, \qquad (8)$$

TABLE 4

CONSTRAINTS ON MOLECULAR GAS IN THE ICM

Cluster[a] (1)	σ_c[b] (mK) (2)	Reference[c] (3)	$c_f(10^{-4})$[d] (4)	N_{los}[e] (5)	Transition[f] (6)
CL 0016+16	1.9	1	2.9	5.8	1 → 0
MKW 1	1.5	2	2.3	3.0	1 → 0
A262	4.1	3	6.2	8.2	1 → 0
2A 0335+096	2.0	2, 3	3.0	4.0	1 → 0
A478	2.3	1	3.5	7.0	1 → 0
A496	2.7	1, 3	4.1	5.4	1 → 0
0745−191	4.3	4	6.5	8.6	1 → 0
A978	4.2	3	6.3	8.4	1 → 0
Hydra A	5.0	4	7.5	10.0	1 → 0
Hydra A	18.0	5	6.8	9.0	2 → 1
A1060	32.3	5	12.2	16.1	2 → 1
A1126	0.5	2, 3	0.8	10.0	1 → 0
A1185	2.8	3	4.2	5.6	1 → 0
M87	11	6	16.5	22.0	1 → 0
NGC 4696	5.2	4	7.8	10.4	1 → 0
NGC 4696	14.0	4	5.3	7.0	2 → 1
A1795	1.9	3	2.9	3.8	1 → 0
MKW 3s	13.9	5	5.3	6.9	2 → 1
A1983	3.3	3	5.0	6.6	1 → 0
A2029	1.9	1	2.9	5.8	1 → 0
A2052	5.9	3	8.9	11.8	1 → 0
A2151	20.3	5	7.7	10.1	2 → 1
A2199	1.3	1, 2, 3	2.0	2.6	1 → 0
A2256	30.9	5	11.7	15.4	2 → 1
A2319	1.9	3	2.9	3.8	1 → 0
Cygnus A	32.6	5	12.3	16.3	2 → 1

[a] Source.

[b] Channel-to-channel rms σ_c in the main beam (Rayleigh-Jeans) brightness temperature. If several values have been reported, the lowest is given.

[c] Reference for σ_c: (1) Antonucci & Barvainis 1993 (using very wide bandwidth); (2) Bregman & Hogg 1988; (3) Grabelsky & Ulmer 1990; (4) This paper; (5) McNamara & Jaffe 1993; (6) Jaffe 1987.

[d] Upper limit on covering factor from eq. (7), assuming a kinetic temperature for the CO of 20 K (see § 6) and converting to Rayleigh-Jeans temperature using eq. (9).

[e] Upper limit on the number of clouds along the line of sight through the cluster (eq. [11]).

[f] The rotational level transition.

where $\Delta V_{ensemble}$ is the total velocity spread in the ensemble of clouds in the ICM and N_{los} is the total number of clouds along the line of sight through the cluster.

The X-ray data by themselves do not constrain the velocity distribution or velocity covering factor of the hypothesized molecular clouds. Thus, a possible scenario is that there are only a few clouds along any line of sight through the cluster. In this case, *at any given velocity in the spectrum*, the covering factor of the clouds within the SEST beam will be much smaller than unity. This will cause us to underestimate the mass of molecular gas.

Based on our calculations of equilibrium temperature in the clouds (§ 6) we adopt a CO kinetic temperature of $T_{CO}^K = 20$ K. We assume that the ^{12}CO 1 → 0 line is optically thick, and that the kinetic temperature is equal to the excitation temperature. Recall the Rayleigh-Jeans temperature is given by

$$T_{CO} = \frac{h\nu}{k}\,(e^{h\nu/kT_{CO}^K} - 1)^{-1} \qquad (9)$$

and the thermal velocity width of an individual cloud is given by

$$\Delta V_{thermal} = 0.04(T_{CO}^K)^{1/2}\ \text{km s}^{-1}\,. \qquad (10)$$

Using the Rayleigh-Jeans temperature in equation (7), the covering factor is given by $c_f \lesssim 1.5 \times 10^{-4}\sigma_c$ where σ_c is in units of mK. Using the observed limits σ_c from Table 4, we estimate an upper limit to the corresponding apparent covering factor which would be required to be consistent with all the nondetections of CO. Assuming a *spatial* covering factor of unity, we find typical upper limits to the covering factor of $c_f \simeq c_{vel} \lesssim 4.5 \times 10^{-4}$. Combining equations (7), (8), (9), and (10), we derive the following conservative upper limit on N_{los}:

$$N_{los}(1 \to 0) < 7.4\left(\frac{\sigma_c}{3\ \text{mK}}\right)\left(\frac{\Delta V_{ensemble}}{1000\ \text{km s}^{-1}}\right) \times \left(\frac{T_{CO}^K}{20\ \text{K}}\right)^{-1/2}[(e^{5.53/T_{CO}^K} - 1)^{-1} - 0.148]^{-1} \qquad (11a)$$

$$N_{los}(2 \to 1) < 5.6\left(\frac{\sigma_c}{20\ \text{mK}}\right)\left(\frac{\Delta V_{ensemble}}{1000\ \text{km s}^{-1}}\right) \times \left(\frac{T_{CO}^K}{20\ \text{K}}\right)^{-1/2}[(e^{11.06/T_{CO}^K} - 1)^{-1} - 0.017]^{-1} \qquad (11b)$$

For a kinetic temperature of 20 K, we obtain typical upper limits of $N_{los} < 6$ and $N_{los} < 10$ for the 1 → 0 and 2 → 1 transitions, respectively (Table 4). However, the velocity width may not be as small as the thermal width (0.076 km s^{-1}). If the line velocity width in the clouds is 1 km s^{-1}, then the upper limit drops to $N_{los} < 0.5$ and $N_{los} < 0.8$ for the 1 → 0 and 2 → 1 transitions, respectively.

We also consider the maximum optical depth permitted in a single cloud, for a given choice of line width and cloud temperature, under the constraint that the cloud must not produce more than the observed column density of hydrogen. The optical depth in the ^{12}CO 1 → 0 and 2 → 1 lines is given by

$$\tau(1 \to 0) = 1.5 \times 10^{-15}\,\frac{\epsilon N_{CO}}{\Delta V_{cloud}}\,(1 - e^{-5.53/T_{ex}})\,, \qquad (12a)$$

$$\tau(2 \to 1) = 1.0 \times 10^{-15}\,\frac{\epsilon N_{CO}}{\Delta V_{cloud}}\,(1 - e^{-11.06/T_{ex}})\,, \qquad (12b)$$

where N_{CO} is the column density of CO molecules, ϵ is the fraction of molecules which are in the lowest rotational level of the transition, and T_{ex} is the excitation temperature of the CO. The total number of clouds N_{los} along the line of sight through the cluster is given by the total column density of hydrogen inferred from the X-ray observations (White et al. 1991) divided by the column density of a "typical" single cloud. Thus, we can write down an expression for the number of clouds of molecular gas along the line of sight which add up to provide the column density of hydrogen inferred by White et al. (1991). To do this, we (1) assume that the ratio of molecular hydrogen to CO is 10^4, (2) express the cloud velocity line width in terms of the thermal line width (eq. [10]), (3) assume the kinetic and excitation temperatures are equal to 20 K (§ 3), and (4) calculate the fraction of molecules in the lowest rotational level of the transition ϵ assuming LTE. This gives the following upper limits based on the 1 → 0 and 2 → 1 lines

$$N_{los}(1 \to 0) < 0.1\left(\frac{\tau}{100}\right)^{-1}\left(\frac{T_{ex}}{20}\right)^{-0.5} \times \left(\frac{\epsilon}{0.13}\right)\left(\frac{N_H}{10^{21}}\right)[1 - e^{-0.28(20/T_{ex})}] \qquad (13a)$$

$$N_{\rm los}(2 \rightarrow 1) < 0.4\left(\frac{\tau}{100}\right)^{-1}\left(\frac{T_{\rm ex}}{20}\right)^{-0.5} \times \left(\frac{\epsilon}{0.32}\right)\left(\frac{N_{\rm H}}{10^{21}}\right)[1 - e^{-0.55(20/T_{\rm ex})}] . \quad (13b)$$

Note that since equations (13a) and (13b) for $N_{\rm los}$ are expressed in terms of the column density of a cloud, they depend on the optical depth of the molecular clouds. Thus with a choice for cloud velocity (we adopt the thermal velocity as a lower limit), kinetic temperature (we adopt 20 K as a lower limit) and $N_{\rm los}$, equations (13a) and (13b) become a constraint on the optical depth of the cloud. If $N_{\rm los}$ is much less than unity, then this is inconsistent with the X-ray absorption (e.g., White et al. 1991; Allen et al. 1993) which requires a spatial covering factor of order unity. If $N_{\rm los}$ is much greater than unity, then this is inconsistent with our constraints from the nondetection of CO in emission which require a low value of $N_{\rm los}$ in order to dilute the CO emission (eq. [11]; Table 4). Thus we have the constraint that $N_{\rm los}$ must be of order unity or slightly larger. We can estimate the optical depth of the CO using equations (13a) and (13b) by making the additional assumption that $N_{\rm los} \sim 1$. Then, $\tau(1 \rightarrow 0) \lesssim 10$ and $\tau(2 \rightarrow 1) \lesssim 40$ (these upper limits are reduced if the line width is greater than the thermal value or if the CO abundance is lower than assumed). These predictions of CO optical depth should be tested.

5.2. *Atomic Hydrogen*

If the gas is primarily atomic, then in order to escape detection in emission by the existing observations of the 21 cm line (Burns, White, & Haynes 1981; Valentijn & Giovanelli 1982; McNamara, Bregman, & O'Connell 1990; O'Dea & Payne 1991, 1993) a necessary condition is that the optical depth in the 21 cm line in each cloud along the line of sight is very large ($\gtrsim 100$, e.g., Jaffe 1992). This gives the requirement

$$\tau \simeq 5 \times 10^{-19} N_{\rm H} T_s^{-1} \Delta V_{\rm cloud}^{-1} > 100 , \quad (14)$$

where T_s is the spin temperature, and $\Delta V_{\rm cloud}$ is the velocity width of the emission line from a single cloud. The smallest possible line width is that given by the thermal width (FWHM)

$$\Delta V_{\rm cloud} \gtrsim 0.24 T_s^{1/2} \text{ km s}^{-1} . \quad (15)$$

The line width can be larger if the cloud has internal turbulence. For example, in our Galaxy, typical observed line widths are a few km s^{-1}. The total number of clouds $N_{\rm los}$ along the line of sight through the cluster is given by the total column density of hydrogen inferred from the X-ray observations divided by the column density of a "typical" single cloud. Combining equations (14) and (15) and the definition of $N_{\rm los}$ and adopting a spin temperature of $T_s = 20$ K (see § 6) gives a conservative upper limit to $N_{\rm los}$

$$N_{\rm los} < 0.2\left(\frac{\tau}{100}\right)^{-1}\left(\frac{T_s}{20}\right)^{-1.5}\left(\frac{N_{\rm H}}{10^{21}}\right) . \quad (16)$$

Thus, the *upper limit* to $N_{\rm los}$ is about unity. If the optical depth is as large as 1000 as suggested by Jaffe (1992) and/or the cloud line width is much larger than the thermal line width (due to turbulence), then the upper limit to the number of clouds along each line of sight is much less than unity. This would be a contradiction since it violates the requirement that the covering factor be of order unity. Note that (as discussed by White et al. 1991 and Jaffe 1992) a small value for $N_{\rm los}$ is *required* in order to dilute the signal due to absorption against the background radio sources and explain the nondetection of H I absorption by, e.g., Shostak et al. (1983), McNamara et al. (1990), and Jaffe (1992). Thus, inconsistent parameters are required for the population of atomic hydrogen clouds, and this is a serious problem for the current explanation for the X-ray absorption.

6. IS THE MOLECULAR GAS VERY COLD?

Another way to explain the nondetections of CO in clusters of galaxies is to make the molecular gas very cold, with kinetic temperature $T_{\rm CO}^K \simeq 2.7$ K. Equation (6) shows that the signal in our spectrum can be considerably reduced if the Rayleigh-Jeans temperature of the CO is very close to that of the 2.7 K background.

In our Galaxy the kinetic temperature of molecular clouds seems to reach a lower limit of around 10 K (Goldsmith 1987) due to a balance between radiative losses and heating by photoelectrons from dust grains and cosmic ray ionization (e.g., Boland & de Jong 1984). Suchkov, Allen, & Heckman (1993) suggest that cosmic rays can heat molecular clouds very efficiently. Given that these cooling flow clusters contain powerful incoherent synchrotron radio sources we may expect cosmic-ray heating to be significant and a similar balance to hold, though this extrapolation is uncertain. The energy density is relativistic *electrons* is typically $u_e \sim 10^{-12}$ to 10^{-11} ergs cm^{-3} (e.g., O'Dea & Baum 1986), which is 1–10 times the energy density of cosmic rays in the solar neighborhood (Jura 1987). As relativistic electrons are not very efficient at heating gas, their contribution to the heating will not be significant for these energy densities. However, presumably there is an associated component of energetic *protons*, which (depending on the energy spectrum and low-energy cutoff) could heat the gas at a rate comparable to or greater than the solar neighborhood cosmic-ray heating rate.

The unobservability of the cosmic-ray protons in clusters make estimates of their contribution to the heating rate necessarily uncertain. Thermal conduction is also a potentially very important heating mechanism, but calculations of the heating rate are plagued by uncertainties in the magnetic field geometry, which could act to suppress conduction (e.g., David, Hughes, & Tucker 1992; Rosner & Tucker 1989; Tribble 1989). However, there is another gas-heating mechanism operating in clusters which can be much better constrained: any cold clouds embedded in the hot intracluster gas will be irradiated by the thermal bremsstrahlung and line emission produced by the hot gas. Hence the clouds will be exposed to a substantial X-ray flux which will both ionize and heat the gas. Here we estimate the X-ray heating rate and compare it to the cooling rate for molecular gas in order to estimate the temperature of such clouds.

6.1. *The X-Ray Heating Rate*

X-ray–luminous clusters typically have gas temperatures $T_h \sim 2$–8 keV, central gas number densities $n_0 \sim 10^{-3}$ cm^{-3}, and gas distributions which can be described tolerably well by the nonsingular isothermal sphere profile

$$n(r) = \frac{n_0}{1 + (r/r_c)^2} \text{ cm}^{-3} , \quad (17)$$

where the core radius $r_c \sim 200$ kpc (e.g., Jones & Forman 1984). In clusters with cooling flows, the inferred density dis-

tribution near the cluster center is somewhat steeper than the isothermal sphere and the central densities tend to be in the range $n_0 \sim 10^{-3}$ to 10^{-2} cm^{-3} (e.g., Stewart et al. 1984). For temperatures $T_h \gtrsim 2$ keV, the emission from the hot gas is dominated by thermal bremsstrahlung; the emissivity for an ion with charge Z and number density n_i in a gas with electron density n_e is (Rybicki & Lightman 1979)

$$\epsilon_\nu^{\rm ff} = 2.4 \times 10^{-16} Z^2 n_e n_i \, T_{\rm keV}^{-1/2} \times e^{-E_{\rm keV}/T_{\rm keV}} \bar{g}_{\rm ff} \text{ keV cm}^{-3} \text{ s}^{-1} \text{ keV}^{-1} \text{ sr}^{-1} \equiv \epsilon_\nu^0 Z^2 n_e n_i \quad (18)$$

where $\bar{g}_{\rm ff}$ is the velocity-averaged Gaunt factor, and both the gas temperature and photon energy are expressed in keV. In the relevant parameter regime, the Gaunt factor is accurately given by $\bar{g}_{\rm ff} \simeq 0.55 \ln(2.25 T_{\rm keV}/E_{\rm keV})$.

In order to make the calculation both simpler and easy to apply, we will consider only the bremsstrahlung emission from the gas, which will provide a lower limit to the X-ray flux and hence to the ionization and heating rates. For the density distribution (17), the bremsstrahlung "flux" (i.e., $4\pi J_E$, where J_E is the mean intensity at energy E) seen by a cloud at a radial distance R from the center of the cluster can be written as

$$4\pi J_E(R) = \frac{1.5\pi n_0^2 r_c^4}{(r_c^2 + R^2)^{3/2}} \epsilon_\nu^0 \times \int_0^\pi F(\theta, b, k)\, d\theta \text{ keV cm}^{-2} \text{ s}^{-1} \text{ keV}^{-1}, \quad (19)$$

where the factor of 1.5 corrects for He and heavy element bremsstrahlung, and $F(\theta, b, k)$ is a somewhat complicated function of spherical polar angle θ, $b = R/R_b$, where R_b is the outer boundary of the cluster gas distribution, and $k = R/(r_c^2 + R^2)^{1/2}$. To adequate approximation, the value of the integral is π; this underestimates the flux at large R ($k \to 1$).

For low ionization fractions ($x_e \lesssim 10^{-2}$), the fraction of a primary photoelectron's energy which goes into secondary ionization is approximately 0.4 (Voit 1991). The number of secondary ionizations of molecular hydrogen produced by a photon of energy $E_{\rm keV} = E/1$ keV is then $\delta\zeta_s \approx 26 E_{\rm keV}$; hence for X-ray–irradiated clouds the secondary ionizations dominate the total ionization rate. The ionization rate per molecule is then

$$\zeta_T \approx 26 \int_{E_{\rm min}}^{E_{\rm max}} 4\pi J_E \sigma_{\rm XR}(E)\, dE \text{ s}^{-1}, \quad (20)$$

where we have ignored the difference between photon and photoelectron energies; $\sigma_{\rm XR}$ is the photoionization cross section per H atom, which we take to be $\sigma_{\rm XR} = \sigma_0 E_{\rm keV}^{-\beta}$, with $\sigma_0 = (6 \times 10^{-23}, 2.6 \times 10^{-22})$ cm^2, $\beta = (3, 8/3)$ for ($E < 0.5$ keV, $E \geq 0.5$ keV), respectively (Morrison & McCammon 1983). $E_{\rm min}$ and $E_{\rm max}$ are the minimum and maximum X-ray energies considered; we take $E_{\rm min} = 100$ eV so that we can ignore any ionized gas column around the clouds and take $E_{\rm max} = 10$ keV. The results are very insensitive to $E_{\rm max}$ for $E_{\rm max} > T_{\rm keV}$.

The X-ray ionization also leads to heating of the gas, as the energetic electrons lose energy through Coulomb losses, excitations, and ionization; in a molecular gas much of the ionization energy goes into gas heating due to dissociative recombination (Glassgold & Langer 1973). We will assume that the fraction of a primary photoelectron's energy which goes into heating $f_h \approx 0.5$. The gas heating rate per molecule (ergs s^{-1}) is then identical in form to equation (20), with the numerical coefficient 26 replaced by f_h. We will also allow for the presence of some attenuating column density $N_{\rm att}$ (i.e., depth dependence within a cloud), by multiplying J_E in equation (20) by $e^{-\tau_0 E^{-\beta}}$, where $\tau_0 = N_{\rm att}\sigma_{\rm XR}$ (at 1 keV). For the clusters studied by White et al. (1991), $N_{\rm att}$ can be no larger than $\sim 10^{21}$ cm^{-2}, i.e., the total absorbing column density inferred from the X-ray spectra. This implies an upper limit to the 1 keV optical depth of $\tau_0 \sim 0.25$. We adopt this value as typical; the results are not very sensitive to the assumed value (see below). The ionization rate (20) can then be written

$$\zeta_T(R) \approx 1.1 \times 10^3 \frac{n_{-3}^2 r_{100}}{(1 + R^2/r_c^2)^{3/2}} 2\sigma_0 T_{\rm keV}^{-1/2} \times 26 \times \int_{E_{\rm min}}^{E_{\rm max}} e^{-\tau_0 E^{-\beta}} \bar{g}_{\rm ff} e^{-E/T} E^{-\beta}\, dE \approx 1.5 \times 10^{-17} \frac{n_{-3}^2 r_{100}}{(1 + R^2/r_c^2)^{3/2}} T_{\rm keV}^{-1/2} \times \int_{E_{\rm min}}^{E_{\rm max}} e^{-\tau_0 E^{-\beta}} \bar{g}_{\rm ff} e^{-E/T} E^{-\beta}\, dE \text{ s}^{-1}, \quad (21)$$

where $r_{100} = r_c/100$ kpc, $n_{-3} = n_0/10^{-3}$ cm^{-3}, and the factor of 2 times σ_0 corrects from the cross section per H atom to cross section per H_2 molecule; E and T are in keV. The integral in equation (21) has been evaluated numerically; a good approximation to the results is

$$\int_{E_{\rm min}}^{E_{\rm max}} e^{-\tau_0 E^{-\beta}} \bar{g}_{\rm ff} e^{-E/T} E^{-\beta} dE \approx \begin{cases} 0.26 T_{\rm keV}^{0.6} \tau_0^{-0.65} & (0.01 \leq \tau_0 \leq 0.5) \\ 0.1 T_{\rm keV} \tau_0^{-1.1} & (0.5 < \tau_0 \leq 2.5) \end{cases}$$

for $E_{\rm min} = 0.1$ keV, $E_{\rm max} = 10$ keV. These expressions are accurate to 20%. Using the above approximation in equation (21) for the ionization rate and the corresponding equation for the X-ray photoionization heating rate then gives

$$\zeta_T(R) \approx 3.9 \times 10^{-18} \frac{n_{-3}^2 r_{100}}{(1 + R^2/r_c^2)^{3/2}} \times T_{\rm keV}^{0.1} \tau_0^{-0.65} \text{ s}^{-1} \quad (0.01 \leq \tau_0 \leq 0.5) \quad (22a)$$

$$\approx 1.5 \times 10^{-18} \frac{n_{-3}^2 r_{100}}{(1 + R^2/r_c^2)^{3/2}} \times T_{\rm keV}^{1/2} \tau_0^{-1.1} \text{ s}^{-1} \quad (0.5 < \tau_0 \leq 2.5) \quad (22b)$$

for the ionization rate and

$$\Gamma_\pi(R) \approx 2.4 \times 10^{-28} \frac{n_{-3}^2 r_{100}}{(1 + R^2/r_c^2)^{3/2}} f_h \times T_{\rm keV}^{0.1} \tau_0^{-0.65} \text{ ergs s}^{-1} \quad (0.01 \leq \tau_0 \leq 0.5) \quad (23a)$$

$$\approx 9.2 \times 10^{-29} \frac{n_{-3}^2 r_{100}}{(1 + R^2/r_c^2)^{3/2}} f_h \times T_{\rm keV}^{1/2} \tau_0^{-1.1} \text{ ergs s}^{-1} \quad (0.5 < \tau_0 \leq 2.5) \quad (23b)$$

for the heating rate. For the default values of all the parameters, the ionization and heating rates are comparable to or larger than the corresponding cosmic-ray rates in molecular clouds in the solar neighborhood (Black 1987).

6.2. *Equilibrium Molecular Cloud Temperatures*

Assuming thermal equilibrium, the gas temperature will be determined by the balance between heating and cooling rates. For the molecular gas cooling function, we have used the

cooling rates calculated by Goldsmith & Langer (1978), which include line cooling from both molecular and atomic species likely to be abundant in molecular clouds. We are thus assuming that the clouds have metallicities similar to solar neighborhood clouds. This was also implicit in our adopted X-ray absorption cross section. The Goldsmith & Langer cooling functions include optically thick species; they assume a velocity gradient of 1 km s^{-1} pc^{-1} in calculating the effects of radiative trapping.

Goldsmith & Langer calculated cooling rates over a wide range of densities and temperatures, and give analytic expressions for the total cooling rate as a function of temperature for a range of densities. The cooling rate per H_2 molecule is actually only weakly dependent on n_{H_2} for densities in excess of a few hundred cm^{-3}, due to collisional deexcitation and the effects of radiative trapping. The cooling rates obtained by Goldsmith & Langer for H_2 densities of 10^3, 10^4, and 10^5 cm^{-3} are

$$n^2\Lambda = 6.8 \times 10^{-27} T^{2.2} \text{ ergs cm}^{-3} \text{ s}^{-1} \quad (24a)$$

$$n^2\Lambda = 1.5 \times 10^{-26} T^{2.7} \text{ ergs cm}^{-3} \text{ s}^{-1} \quad (24b)$$

$$n^2\Lambda = 3.8 \times 10^{-26} T^{2.9} \text{ ergs cm}^{-3} \text{ s}^{-1}, \quad (24c)$$

where Λ is the cooling function (ergs cm^3 s^{-1}). Note that if the amount of turbulence in the cloud is less than that assumed by Goldsmith & Langer, then the cooling becomes less efficient and the resulting temperatures will be higher.

Consider first the case with $\tau_0 \leq 0.25$. Equating the heating rate (23a) and the cooling rates (24), $n\Gamma_\pi = n^2\Lambda$, and solving for the temperature, we obtain

$$T = 5.6\left[\frac{n_{-3}^2 r_{100}}{(1 + R^2/r_c^2)^{3/2}}\right]^{0.45} f_{0.5}^{0.45} T_{\text{keV}}^{0.045} \tau_{0.25}^{-0.30} \text{ K}; \quad (25a)$$

$$T = 7.1\left[\frac{n_{-3}^2 r_{100}}{(1 + R^2/r_c^2)^{3/2}}\right]^{0.37} f_{0.5}^{0.37} T_{\text{keV}}^{0.037} \tau_{0.25}^{-0.24} \text{ K}; \quad (25b)$$

$$T = 10.0\left[\frac{n_{-3}^2 r_{100}}{(1 + R^2/r_c^2)^{3/2}}\right]^{0.34} f_{0.5}^{0.34} T_{\text{keV}}^{0.034} \tau_{0.25}^{-0.22} \text{ K}; \quad (25c)$$

for densities $n_{H_2} = (10^3, 10^4, 10^5)$ cm^{-3}, where $f_{0.5} = f_h/0.5$ and $\tau_{0.25} = \tau_0/0.25$. Equations (25) can be put in a more compact form by writing them as

$$T = T_0\left[\frac{n_{-3}^2 r_{100}}{(1 + R^2/r_c^2)^{3/2}}\right]^a f_{0.5}^a T_{\text{keV}}^{0.1a} \tau_{0.25}^{-0.65a} \quad (26)$$

with $T_0 = (5.6, 7.1, 10.0)$ K, $a = (0.45, 0.37, 0.34)$ for $n_{H_2} = (10^3, 10^4, 10^5)$ cm^{-3}, respectively. Note that the density dependence has been dropped, as it would imply a scaling of temperature with n_{H_2} which is incorrect, as is obvious from comparison of equations (25a)–(25c).

The analog of equation (26) for the higher optical depth case, with heating rate given by equation (23b), is

$$T = T_0\left[\frac{n_{-3}^2 r_{100}}{(1 + R^2/r_c^2)^{3/2}}\right]^a f_{0.5}^a T_{\text{keV}}^{0.5a} \tau_{1.0}^{-1.1a} \quad (27)$$

with $T_0 = (2.4, 3.6, 5.2)$ K for $n_{H_2} = (10^3, 10^4, 10^5)$ cm^{-3}. The values of a are the same as equation (26).

To estimate the cloud temperatures, we need the hot gas parameters (n_0, T_h, r_c) for the clusters of interest; these can be obtained from studies of the X-ray emission. Since these parameters are usually determined from fits to the large-scale gas distributions in the clusters (i.e., outside the cooling radius) clusters with cooling flows will have gas which is both denser and cooler than implied by the X-ray fits in their cores. Since this gas will radiate more strongly than we are assuming here, we are again underestimating the actual X-ray fluxes which will be seen by a cloud, and hence the cloud temperatures. For the Hydra A cluster, David et al. (1990) find $T_{\text{keV}} \approx 4.5$, $n_{-3} \approx 6.5$, and $r_{100} = 1.45$. For the Centaurus cluster, Matilsky et al. (1985) obtain $T_{\text{keV}} \approx 2.1$, $n_{-3} \approx 9$, and $r_{100} \approx 2$. Arnaud et al. (1987) derive $T_{\text{keV}} \approx 8.6$, $n_{-3} \approx 35$, and $r_{100} \approx 0.5$ for PKS 0745−191.

Using equations (25) (which is really the only choice consistent with the inferred absorbing column densities), we estimate minimum molecular cloud temperatures in the range 30–50 K at 100 kpc from the cluster center (Table 5). Since the thermal pressures inferred in the cores of these clusters are $P/k \sim 10^5$–10^6 cm^{-3} K (Heckman et al. 1989), at these temperatures the cloud densities must be $\sim 10^4$–10^5 cm^{-3} for the clouds to be in pressure equilibrium with the hot gas. The cooling function for $n_{H_2} = 10^5$ cm^{-3} always produces the highest temperatures; due to collisional deexcitation, increasing the density still further will generally raise the temperatures.

These temperatures, which we emphasize will be lower limits to the actual gas kinetic temperatures, are clearly much too high for temperature effects to explain the nondetections of cooling flow clusters discussed in this paper. Note that if the clouds remain cold by shielding themselves from the X-ray photons because of very large optical depth, this causes two additional problems: (1) The total amount of molecular mass required is substantially increased, and (2) it becomes difficult to reconcile the X-ray observations with the inferred spatial covering factor of order unity. In fact, even fairly substantial increases in the 1 keV optical depth of the clouds produce only

TABLE 5

MINIMUM EQUILIBRIUM TEMPERATURES

Cluster[a] (1)	n_{H_2}[b] (cm^{-3}) (2)	τ_0[c] (3)	$T_{R=100}$[d] (K) (4)	$T_{R=200}$[e] (K) (5)
Hydra A	10^3	0.25	29	19
Hydra A	10^4	0.25	28	19
Hydra A	10^5	0.25	35	25
Hydra A	10^3	1.0	17	11
Hydra A	10^4	1.0	18	12
Hydra A	10^5	1.0	22	16
Centaurus A	10^3	0.25	49	36
Centaurus A	10^4	0.25	44	33
Centaurus A	10^5	0.25	53	41
Centaurus A	10^3	1.0	24	18
Centaurus A	10^4	1.0	24	19
Centaurus A	10^5	1.0	30	23
PKS 0745−191	10^3	0.25	37	16
PKS 0745−191	10^4	0.25	34	17
PKS 0745−191	10^5	0.25	42	23
PKS 0745−191	10^3	1.0	24	10
PKS 0745−191	10^4	1.0	24	12
PKS 0745−191	10^5	1.0	29	18

[a] Cluster name.
[b] Number density of molecular hydrogen.
[c] τ_0 is the optical depth at 1 keV due to photoelectric absorption.
[d] The minimum equilibrium temperature of the molecular gas at a radius of 100 kpc.
[e] The minimum equilibrium temperature of the molecular gas at a radius of 200 kpc.

modest reductions in the cloud temperature. This results from the relatively weak decline of the X-ray heating rate with optical depth and the strong temperature dependence of the cooling functions (24). (This also implies that the precise value of f_h is not important: reducing it by an order of magnitude would only lower the temperatures by about a factor of 2 for $n_{H_2} \geq 10^4$ cm^{-3}.) Using the temperature equation (27) for $\tau_0 = 1.0$ produces similar, though slightly lower minimum molecular cloud temperatures (Table 5). Furthermore, substantial temperature gradients would be present in clouds with such high optical depths, and the CO emission (if optically thick) would be weighted by the outer, hotter regions of the clouds.

6.3. *Effects of Varying Metallicity*

The effect of changing the metallicity on the temperature depends on precisely what the heating and cooling agents are. In the case of interest here, with heating provided by X-rays and cooling by molecular and atomic species, we expect the equilibrium cloud temperatures will be insensitive to even fairly substantial changes in the gas phase abundances.

In general, the CO cooling will be dominated by the highest rotational (J) levels that are fairly well populated; these levels usually have moderate optical depths. Thus, raising or lowering the metallicity will raise or lower the total cooling (usually less than linearly with metallicity), even though the lower J levels (such as $J = 1$ and 2) may be quite optically thick, so that the emergent intensity in those low-J lines is insensitive to their actual optical depths. Many of the additional coolants that are likely to be important in these clouds, such as the C I fine-structure lines and the rare isotopes of CO, will ordinarily be optically thin, so that the cooling from these species will scale directly with the metallicity. Thus the total gas cooling will vary roughly linearly with the gas-phase metallicity. For the X-ray heating discussed here, the absorption cross section will scale linearly with abundance, so that the heating rate will also. We therefore do not expect a strong dependence of the equilibrium temperature on the precise gas phase abundances.

Given the substantial temperatures which we infer for the clouds, the only other way to explain our nondetections is for the CO emission from the clouds to be quite optically thin, e.g., by analogy with diffuse molecular clouds in the Galaxy, where the CO abundance is typically of order 10^{-6}. However, these clouds also tend to have atomic hydrogen column densities which are comparable to or greater than their molecular hydrogen column densities. At the considerably higher densities and lower UV fluxes (compared to Galactic diffuse clouds) that would be seen by clouds in these clusters, it is possible that the transition to fully molecular will occur at smaller total column densities. However, since gas-phase chemical reactions involving the molecular ion H_3^+ provide a very rapid route for formation of molecules like CO, it is difficult to see how these clouds could have most of their hydrogen in molecular form and yet have very small abundances of other molecules. Since the ionization rates (and hence electron fractions) in these clouds are expected to be comparable to Galactic molecular clouds (§ 6.1), a large fractional abundance of H_2 will inevitably drive much of the carbon and oxygen into molecules such as CO under these conditions.

6.4. *The Relationship between Gas and Dust Temperatures*

Bregman (1992) reviews evidence for the existence of dust in the ICM of cooling flow clusters (Hu 1988; Bregman, McNamara, & O'Connell 1990; Grabelsky & Ulmer 1990; Wise et al. 1993). *IRAS* detections at 100 and 60 μm suggest the presence of dust at temperatures of 20–30 K. For a dust temperature of 30 K, the mean mass of dust within a 4′ aperture is $10^{7.5}$ $M_\odot$ and for the entire cluster is $10^{10.3}$ $M_\odot$ (Wise et al. 1993). Note that Annis & Jewitt (1993) report nondetections of thermal emission from dust in the submillimeter. Their upper limits of $\sim 10^8$ $M_\odot$ of dust within the 16″–18″ JCMT beam are *just* consistent with the *IRAS* detections. Bregman (1992; cf. Sparks & Cameron 1988) suggests that the dust is heated by collisions with the 10^7 K electrons which emit the detected X-rays (Dwek, Rephaeli, & Mather 1990). We note the dust temperatures estimated by Bregman are in good agreement with our estimated equilibrium temperature for the molecular gas. This could be either coincidental or a reflection of some physical connection.

If Bregman's model is to be applied to dust in molecular clouds (rather than dust grains in situ in the hot intracluster gas), it requires that the mean free path of a 10^7 K electron is comparable to or larger than the size of the clouds which contain the dust.[5] This constrains the clouds to be very small (much less than a parsec), in agreement with the estimates of Loewenstein & Fabian (1990) and White et al. (1991). If this is the case, there may be a simple connection between the dust and gas temperatures, with the gas heating provided by the dust. Once the gas densities get above roughly 10^4 cm^{-3}, energy transfer between the dust and gas at these temperatures (a few tens of K) becomes quite efficient, so that the dust temperature and gas kinetic temperature approach equality. Thus, if the gas densities are high enough, the gas is heated by the dust, which is in turn heated by the hot electrons from the ICM. (Note that the dust is radiating far more energy than the gas, so that dust cooling dominates the energy budget of the clouds.) In equilibrium, the temperatures are equal, or nearly so. In this case the gas temperature is determined by the dust temperature, although we find that the gas temperatures should be of the same order even neglecting heating by the dust.

A possible problem with Bregman's model is that it requires the energy losses of the hot gas to dust heating to be an order of magnitude larger than the X-ray radiation losses (at least for the *IRAS*-detected clusters), so that the dust losses dominate the hot gas energetics. However, Dwek et al. (1990) modeled the heating of dust by the hot ICM and found that the losses to dust heating (at least for the Coma Cluster) are not important. This argues that some other process must be responsible for heating the dust seen by *IRAS*. In this case the observed dust may have nothing to do with clouds heated by the intracluster gas, and the similarity of the dust temperatures to our calculated gas temperatures is coincidental. If the gas to dust ratio in the ICM is $\gtrsim 100$, then the estimated dust mass in the cluster of $\sim 10^{10}$ $M_\odot$ (Wise et al. 1993) corresponds to a gas mass of $\gtrsim 10^{12}$ $M_\odot$. However, this much gas at temperatures of 20–30 K seems ruled out by our results. Thus, the picture is likely to be more complicated than considered so far.

7. CONCLUSIONS

We report on the results of a search for molecular gas in a heterogeneous sample of radio loud galaxies using the SEST 15

[5] If the cloud size becomes much smaller than the electron mean free path, then momentum transfer between the hot gas and the cloud becomes inefficient, and it becomes difficult to pressure-confine the clouds. In this case, the clouds must be gravitationally bound.

m millimeter-wavelength telescope in Chile. Observations of ^{12}CO $J = 1 \rightarrow 0$ were obtained of NGC 4696 (PKS 1246−41), the dominant galaxy in the Centaurus cluster, two other rich cooling flow clusters PKS 0745−191 and Hydra A (3C 218, PKS 0915−11, Abell 780), and two powerful radio galaxies PKS 0634−206 and PKS 1934−638. Observations of ^{12}CO $J = 2 \rightarrow 1$ were also obtained of NGC 4696.

We do not detect CO in emission in any of the cluster sources at a 3 σ level of typically 15 mK. White et al. (1991) have suggested that the apparent low-energy X-ray absorption toward cooling flow clusters is due to column densities of $N_H \sim 10^{21}$ cm^{-2} in these clusters with a spatial covering factor of order unity and a total mass of $M \sim 10^{12}\ M_\odot$. Our limits are inconsistent with these column densities and spatial covering factor unless the molecular gas is very cold (kinetic temperature close to 2.7 K) or there only a few clouds along each line of sight. We calculate the heating by X-rays from the intracluster medium and derive constraints on the equilibrium temperatures of the molecular clouds. We estimate *minimum* temperatures in the range ~20–30 K. (We note that the dust temperatures estimated by Bregman 1992 are in good agreement with our gas temperatures, though this may be a coincidence). These calculations suggest that it is not possible to cool the clouds sufficiently to explain the nondetections of molecular gas as a result of low temperature (kinetic temperature close to 2.7 K).

We find that clouds of atomic and molecular hydrogen require strict fine-tuning of parameter space in order to satisfy the requirements for the large column densities $N_H \sim 10^{21}$ cm^{-2}, unity covering factor, and a small number of clouds along the line of sight. The combination of these constraints with the additional requirement that the optical depth in H I be very large is inconsistent with the clouds being atomic. Clouds of molecular hydrogen are not currently ruled out, but the range of parameter space is shrinking. Currently the only way molecular gas can be responsible for the X-ray absorption and still be consistent with our observations is if (1) there is of order one cloud along the line of sight and (2) the optical depth in ^{12}CO $1 \rightarrow 0$ is less than 10.

We present a VLA image of NGC 4696 which shows a diffuse radio morphology comparable to that of the dust lane and emission line complex and suggest this object is a member of the class of "amorphous cooling flow radio sources."

Two blueshifted ^{12}CO $1 \rightarrow 0$ absorption features are tentatively detected toward Hydra A. The nature of the absorbing material is currently unknown, but could be associated with (as yet) unseen galaxies or molecular clouds in the ICM.

^{12}CO $1 \rightarrow 0$ is detected in emission in PKS 0634−206, a classical double radio galaxy which is rich in extended optical emission-line gas. The estimated molecular gas mass is $M_{mol} \sim 3 \times 10^9\ M_\odot$ and is much larger than that of the ionized component detected in Hα, suggesting that the emission line nebula is radiation bounded.

We are grateful to Ger de Bruyn, Harry Payne, Craig Sarazin, and Anatoly Suchkov for helpful discussions, and Greg Taylor for comments on the manuscript. We are grateful to the staff of the SEST for assistence with the observations. SEST is operated jointly by ESO and the Swedish Science Research Council (NFR). Philip Maloney is supported by the NASA Astrophysical Theory Program at the University of Colorado under grant NAGW-766.

REFERENCES

Allen, S. W., Fabian, A. C., Johnstone, R. M., White, D. A., Daines, S. J., Edge, A. C. & Stewart, G. C. 1993, MNRAS, 262, 901
Annis, J., & Jewitt, D. 1993, MNRAS, 264, 593
Antonucci, R., & Barvainis, R. 1993, preprint
Arnaud, K. A., Johnstone, R. M., Fabian, A. C., Crawford, C. S., Nulsen, P. E. J., Shafer, R. A., & Mushotzky, R. F. 1987 MNRAS, 227, 241
Baum, S. A. 1992, in Clusters and Superclusters of Galaxies, ed. A. C. Fabian (Dordrecht: Kluwer), 171
Baum, S. A., & Heckman, T. 1989, ApJ, 336, 681
Baum, S. A., Heckman, T. M., Bridle, A., van Breugel, W., & Miley, G. 1988, ApJS, 68, 643
Baum, S. A., Heckman, T., & van Breugel, W. 1990, ApJS, 74, 389
———. 1992, ApJ, 389, 208
Baum, S. A., & O'Dea, C. P. 1991, MNRAS, 250, 737
Baum, S. A., O'Dea, C. P., & Sarazin, C. L. 1994, in preparation
Black, J. H. 1987, in Interstellar Processes, ed. D. J. Hollenbach & H. A. Thronson (Dordrecht: Reidel), 731
Bloemen, J. B. G. M., et al. 1986, A&A, 154, 25
Böhringer, H., Schwarz, R. A., Briel, U. G., Voges, W., Ebeling, H., Hartner, G., & Cruddace, R. G. 1992, in Clusters and Superclusters of Galaxies, ed. A. C. Fabian (Dordrecht: Kluwer), 71
Boland, W., & de Jong, T. 1984, A&A, 134, 87
Booth, R. S., et al. 1989, A&A, 216, 315
Bregman, J. N. 1992, in Clusters and Superclusters of Galaxies, ed. A. C. Fabian (Dordrecht: Kluwer), 119
Bregman, J. N., & Hogg, D. E. 1988, AJ, 96, 455
Bregman, J. N., McNamara, B. R., & O'Connell, R. W. 1990, ApJ, 351 406
Burns, J. O. 1990, AJ, 99, 14
Burns, J. O., Sulkanen, M. E., Gisler, G. R., & Perley, R. 1992, ApJ, 388, L49
Burns, J. O., White, R. A., & Haynes, M. P. 1981, AJ, 86, 1120
Canizares, C. R., Markert, T. H., & Donahue, M. E. 1988, in Cooling Flows in Clusters and Galaxies, ed. A. C. Fabian (Dordrecht: Reidel), 63
Canizares, C. R., Markert, T. H., Markoff, S., & Hughes, J. P. 1993, ApJ, 405, L17
David, L. P., Arnaud, K. A., Forman, W., & Jones, C. 1990, ApJ, 356, 32
David, L. P., Hughes, J. P., & Tucker, W. H. 1992, ApJ, 394, 452
Davies, R. L., Burnstein, D., Dressler, A., Faber, S. M., Lynden-Bell, D., Terlevich, R., & Wegner, G. 1987, ApJS, 64, 581
Dawe, J. A., Dickens, R. J., & Peterson, B. A. 1977, MNRAS, 178, 675
de Jong, T., Norgaard-Nielsen, H. U., Jorgensen, H. E., & Hansen, L. 1990, A&A, 232, 317
Downes, D. 1989, in Introductory Courses in Galaxies: Evolution of Galaxies, Astronomical Observations, ed. I. Appenzeller, H. Habing, & P. Lena (Heidelberg: Springer-Verlag), 351
Dwek, E., Rephaeli, Y., & Mather, J. 1990, ApJ, 350, 104
Fabian, A. C. 1992, in Clusters and Superclusters of Galaxies, ed. A. C. Fabian (Dordrecht: Kluwer), 151
Fabian, A. C., et al. 1985, MNRAS, 216, 923
Fabian, A. C., Atherton, P. D., Taylor, K., & Nulsen, P. E. J. 1982a, MNRAS, 201, 17P
Fabian, A. C., Hu, E. M., Cowie, L. L., & Grindlay, J. 1981, ApJ, 248, 47
Fabian, A. C., Nulsen, P. E. J., & Canizares, C. R. 1982b, MNRAS, 201, 933
———. 1984, Nature, 310, 733
———. 1991, A&A Rev., 2, 191
Fanti, R., Fanti, C., Schilizzi, R. T., Spencer, R. E., Rendong, N., Parma, P., van Breugel, W., & Venturi, T. 1990, A&A, 231, 333
Fosbury, R. A. E., Bird, M. C., Nicholson, W., & Wall, J. V. 1987, MNRAS, 225, 761
Glassgold, A. E., & Langer, W. D. 1973, ApJ, 186, 859
Goldsmith, P. F. 1987, in Interstellar Processes, ed. D. Hollenbach & H. Thronson (Dordrecht: Reidel), 51
Goldsmith, P. F., & Langer, W. D. 1978, ApJ, 222, 881
Gopal-Krishna, Patnaik, A. R., & Steppe, H. 1983, A&A, 123, 107
Grabelsky, D. A., & Ulmer, M. P. 1990, ApJ, 355, 401
Hansen, L. 1989, in Extranuclear Activity in Galaxies, ed. E. J. A. Meurs & R. A. E. Fosbury (Garching: ESO), 3
Hansen, L., Nørgaard-Nielsen, H. U., & Jørgensen, H. E. A&AS, 71, 465
Harnett, J. I. 1987, MNRAS, 227, 887
Heckman, T., Baum, S., van Breugel, W., & McCarthy, P. 1989, ApJ, 338, 48
Heckman, T. M., Smith, E. P., Baum, S. A., van Breugel, W. J. M., Miley, G. K., Illingworth, G. D., Bothun, G. D., & Balick, B. 1986, ApJ, 311, 526
Hodges, M. W., & Mutel, R. L. 1987, in Superluminal Radio Sources, ed. J. A. Zensus & T. J. Pearson (Cambridge: Cambridge Univ. Press), 168
Hu, E. M. 1988, in Cooling Flows in Clusters and Galaxies, ed. A. C. Fabian (Dordrecht: Kluwer), 73
Jaffe, W. 1987, A&A, 171, 378
———. 1992, in Clusters and Superclusters of Galaxies, ed. A. C. Fabian (Dordrecht: Kluwer), 109
Jauncey, D. L., White, G. L., Batty, M. J., & Preston, R. A. 1986, AJ, 92, 1036
Jedrzejewski, R. I. 1985, PhD thesis, Cambridge Univ.
Jenkins, C. R. 1983, MNRAS, 205, 1321
Johnstone, R. M., Fabian A. C., & Nulsen, P. E. J. 1987, MNRAS, 224, 75

Jones, C., & Forman, W. 1984, ApJ, 276, 38
Jorgensen, H. E., Norgaard-Nielsen, H. U., Pedersen, H., Rasmussen, I. L., & Schnopper, H. 1983, A&A, 122, 301
Jura, M. 1987, in Interstellar Processes, ed. D. J. Hollenbach & H. A Thronson (Dordrecht: Reidel), 3
Kato, T., Tebara, H., Inoue, M., & Aizu, K. 1987, Nature, 329, 223
Kellerman, K. I. 1986, Australian J. Phys., 19, 195
Kronberg, P. P., Wielebinski, R., & Graham, D. A. 1986, A&A, 169, 63
Kühr, H., Witzel, A., Pauliny-Toth, I. I. K., & Nauber, U. 1981, A&AS, 45, 367
Kutner, M. L., & Ulich, B. L. 1981, ApJ, 250, 341
Lazareff, B., Castets, A., Kim, D. W., & Jura, M. 1989, ApJ, 336, L13
Loewenstein, M., & Fabian, A. C. 1990, MNRAS, 242, 120
Maloney, P., & Black, J. H. 1988, ApJ, 325, 389
Matilsky, T., Jones, C., & Forman, W. 1985, ApJ, 291, 621
Mazzarella, J. M., Graham, J. R., Sanders, D. B., & Djorgovski, S. 1993, ApJ, 409, 170
McNamara, B. R., Bregman, J. N., & O'Connell, R. W. 1990, ApJ, 360, 20
McNamara, B. R., & Jaffe, W. 1993, A&A, in press
Mirabel, I. F., Sanders, D. B., & Kazés, I. 1989, ApJ, 340, L9
Miyaji, T., et al. 1993, ApJ, 419, 66
Morrison, R., & McCammon, D. 1983, ApJ, 270, 119
Mushotzky, R. F. 1992, in Clusters and Superclusters of Galaxies, ed. A. C. Fabian (Dordrecht: Kluwer), 91
Mushotzky, R. F., & Szymkowiak, A. E. 1988, in Cooling Flows in Clusters and Galaxies, ed. A. C. Fabian (Dordrecht: Reidel), 53
Noordam, J., & de Bruyn, A. G. 1982, Nature, 399, 598
Norgaard-Nielsen, H. U., & Jorgensen, H. E. 1984, Phys. Scripta, T7, 174
O'Dea, C. P., & Baum, S. A. 1986, in Radio Continuum Processes in Clusters of Galaxies, ed. C. P. O'Dea & J. M. Uson (Green Bank: NRAO), 141
———. 1987, AJ, 94, 1476
O'Dea, C. P., Baum, S. A., & Stanghellini, C. 1991, ApJ, 380, 66
O'Dea, C. P., & Payne, H. 1991, BAAS, 23, 1338
———. 1993, in preparation
Peacock, J. A., & Wall, J. V. 1982, MNRAS, 198, 843
Pedlar, A., Ghataure, H. S., Davis, R. D., Harrison, B. A., Perley, R., Crane, P. C., & Unger, S. W. 1990, MNRAS, 246, 477
Phillips, R. B., & Mutel, R. L. 1982, A&A, 106, 21
Rybicki, G. B., & Lightman, A. P. 1979, Radiative Processes in Astrophysics (New York: Wiley)
Romanishin, W. 1987, ApJ, 323, L113
Rosner, R., & Tucker, W. 1989, ApJ, 338, 761
Sadler, E. M. 1987, in IAU Symp. 127, The Structure and Dynamics of Elliptical Galaxies, ed. T. de Zeeuw (Dordrecht: Reidel), 125
Sadler, E. M., Jenkins, C. R., & Kotanyi C. G. 1989, MNRAS, 240, 591
Sage, L. J., & Isbell, D. W. 1991, A&A, 247, 320
Sarazin, C. L. 1988, X-ray Emission from Clusters of Galaxies (Cambridge: Cambridge Univ. Press)
Sarazin, C. L., & O'Connell, R. W. 1983, ApJ, 268, 552
Schilizzi, R. T., & McAdam, W. B. 1975, MmRAS, 79, 1
Scoville, N. Z., & Sanders, D. B. 1987, in Interstellar Processes, ed. D. Hollenbach & H. Thronson, (Dordrecht: Reidel), 21
Shostak, G. S., van Gorkom, J. H., Ekers, R. D., Sanders, R. H., Goss, W. M., & Cornwell, T. J. 1983, A&A, 119, L3
Simkin, S. M. 1979, ApJ, 234, 56
Smith, E. P., & Heckman, T. M. 1989, ApJS, 69, 365
Sparks, W. B. 1992, ApJ, 399, 66
Sparks, W. B., & Cameron, A. C. 1988, MNRAS, 232, 215
Sparks, W. B., Macchetto, F., & Golombek, D. 1989, ApJ, 345, 153
Stewart, G. C., Fabian, A. C., Jones, C., & Forman, W. 1984, ApJ, 285, 1
Suchkov, A., Allen, R. J., & Heckman, T. M. 1993, ApJ, 413, 542
Tadhunter, C. N., Fosbury, R. A. E., & Quinn, P. J. 1989, MNRAS, 240, 225
Taylor, G. B., & Perley, R. A. 1993, ApJ, 416, 554
Taylor, G. B., Perley, R. A., Inoue, M., Kato, T., Tabara, H., & Aizu, K. 1990, ApJ, 360, 41
Thomas, P. A., Fabian, A. C., & Nulsen, P. E. J. 1987, MNRAS, 228, 973
Tribble, P. C. 1989, MNRAS, 238, 1247
Tzioumis, A. K., et al. 1989, AJ, 98, 36
Ulich, B. L., & Haas, R. W. 1976, ApJS, 30, 247
Valentijn, E. A., & Giovanelli, R. 1982, A&A, 114, 208
van Breugel, W. J. M. 1988, in Hotspots in Extragalactic Radio Sources, ed. K. Meisenheimer & H.-J. Röser (Berlin: Springer-Verlag), 121
Voit, G. M. 1991, ApJ, 377, 158
Wang, Q., & Stocke, J. T. 1993, ApJ, 408, 71
Westbury, C. F., & Henriksen, R. N. 1992, ApJ, 388, 64
White, D. A., Fabian, A. C., Johnstone, R. M., Mushotzky, R. F., & Arnaud, K. A. 1991 MNRAS, 252, 72
White, R. E., III, & Sarazin, C. L. 1987, ApJ, 318, 612
Wills, B. J. 1975, Australian J. Phys. Ap. Suppl., 38, 1
Wise, M. W., O'Connell, R. W., Bregman, J. N., & Roberts, M. S. 1993, ApJ, 405, 94
Young, J. S., & Scoville, N. Z. 1991, ARA&A, 29, 581
Zhao, J.-H., Sumi, D. M., Burns, J. O., Duric, N. 1993, ApJ, 416, 51